Frontiers in Bioscience Landmark

Front. Biosci. (Landmark Ed) **2026**; 31(11): 57611
https://doi.org/10.31083/FBL57611

Original Research

A Novel MMP-3–Targeting Nanobody Potently Suppresses Triple-Negative Breast Cancer Cell Invasion

Alexandra M. Dimesa[1], Alexandra Hockla[1], Mathew A. Coban[1], Derek C. Radisky[1], Evette S. Radisky[1], Alireza Shoari[1,*]

[1]Department of Cancer Biology, Mayo Clinic, Jacksonville, FL 32224, USA
*Correspondence: shoari.alireza@mayo.edu (Alireza Shoari)
Academic Editor: Nikos Karamanos
Submitted: 31 August 2026 Revised: 1 October 2026 Accepted: 13 October 2026 Published: 13 November 2026

Abstract

Background: Matrix metalloproteinase-3 (MMP-3) contributes to extracellular matrix remodeling and has been implicated in breast cancer invasion and metastatic progression. Previous broad-spectrum MMP inhibitors have been limited by inadequate target selectivity and toxicity, highlighting the need for more precise protease-targeting strategies. We sought to identify an MMP-3-targeting nanobody and determine whether inhibition of MMP-3 could suppress invasion in a triple-negative breast cancer (TNBC) cell model. **Methods:** A synthetic nanobody yeast surface display library was screened against the catalytic domain of human MMP-3 using magnetic-activated cell sorting followed by fluorescence-activated cell sorting. Candidate nanobodies were characterized by competitive binding and concentration-dependent affinity measurements. The lead nanobody, NbM3-15, was expressed in soluble form and evaluated in fluorogenic MMP-3 inhibition assays. *MMP3* expression was assessed across TNBC cell lines, and the functional contribution of MMP-3 to the invasion of MDA-MB-436 cells was examined using shRNA-mediated knockdown and Matrigel Transwell assays. NbM3-15 was tested at concentrations of 100–400 nM for inhibition of MDA-MB-436 cell invasion. **Results:** Three rounds of fluorescence-activated cell sorting enriched the MMP-3-binding population from 17.9% to 53.4%, and sequencing identified ten unique nanobody clones. Competition with the engineered MMP-3 inhibitor TIMP-1-C4 reduced MMP-3 binding by all ten candidates, supporting engagement of overlapping sites near the active-site region. NbM3-15 bound MMP-3 with an apparent dissociation constant of 1.26 nM. In solution, NbM3-15 showed time-dependent inhibition, with near-complete suppression of MMP-3 activity after approximately 120 min, and a K_i of 1.64 ± 0.1 nM. MDA-MB-436 cells exhibited the highest *MMP3* transcript levels among the TNBC cell lines examined, and *MMP3* knockdown in this cell line significantly reduced invasion. NbM3-15 likewise suppressed invasion in a dose-dependent manner, with significant inhibition at 200 and 400 nM. **Conclusions:** These findings establish a functional contribution of MMP-3 to invasion in MDA-MB-436 cells, a model of TNBC, and identify NbM3-15 as a potent MMP-3-targeting nanobody with anti-invasive activity. This study provides proof of principle for nanobody-based inhibition of MMP-3 and supports further selectivity, structural, and *in vivo* evaluation of NbM3-15 as a protease-targeted therapeutic strategy.

Keywords: matrix metalloproteinase 3; triple negative breast neoplasms; single-domain antibodies; neoplasm invasiveness; matrix metalloproteinase inhibitors

1. Introduction

Breast cancer remains one of the most frequently diagnosed malignancies worldwide and is a leading cause of cancer-related mortality among women [1]. Despite substantial advances in early detection and treatment, certain molecular subtypes continue to pose major therapeutic challenges [2]. Triple-negative breast cancer (TNBC), defined by the absence of estrogen receptor, progesterone receptor, and HER2 expression, accounts for a particularly aggressive subset of breast cancers characterized by high rates of recurrence, early metastatic dissemination, and limited targeted treatment options [3]. In contrast to hormone receptor-positive or HER2-amplified disease, targeted treatment options for TNBC remain limited, making the identification of new mechanisms that drive tumor progression and invasion especially important [4]. Because metastatic spread remains the principal cause of death in patients with breast cancer, understanding and therapeutically targeting the molecular determinants of tumor invasion is a priority in TNBC research [5].

Tumor invasion is a complex and multistep process that depends not only on intrinsic properties of cancer cells but also on dynamic interactions with the extracellular matrix (ECM) and surrounding stromal microenvironment [6]. To invade adjacent tissues and eventually metastasize, cancer cells must overcome structural barriers imposed by the ECM and basement membrane [7]. This process is facilitated in part by proteolytic enzymes that remodel the tumor microenvironment and enable cell migration [8]. Among these, matrix metalloproteinases (MMPs) have long been recognized as key mediators of cancer progression because of their ability to degrade ECM components, process bioactive molecules, and modulate signaling pathways linked to invasion, angiogenesis, and metastasis [9,10,11]. Dysregu-

Copyright: © 2026 The Author(s). Published by IMR Press.
This is an open access article under the CC BY 4.0 license.

Publisher's Note: IMR Press stays neutral with regard to jurisdictional claims in published maps and institutional affiliations.

lated MMP activity has been reported in many tumor types, including breast cancer, where it contributes to aggressive behavior and poor clinical outcome [12,13].

Within the MMP family, matrix metalloproteinase-3 (MMP-3), also known as stromelysin-1, has attracted attention because of its broad substrate repertoire and its multifunctional role in tumor-associated tissue remodeling [14]. MMP-3 can degrade a variety of ECM proteins and can also activate other proteases, thereby amplifying proteolytic cascades within the tumor microenvironment [15]. In breast cancer, MMP-3 has been implicated in multiple processes associated with tumor progression, including epithelial transformation, invasion, epithelial–mesenchymal transition, and genomic instability [16,17,18,19,20,21]. Beyond its matrix-remodeling activity, MMP-3 may promote malignant behavior by disrupting cell–cell and cell–matrix interactions and by generating a microenvironment that supports tumor initiation and invasion [12,22,23]. MMP-3 may contribute to breast cancer progression not only through direct extracellular matrix remodeling but also by activating other tumor-promoting proteases. MMP-3 has been shown to activate proMMP-9 through sequential cleavage, generating a proteolytically active form of MMP-9 [24]. This mechanistic connection is particularly relevant to basal-like TNBC, as our previous work demonstrated that tumor-cell-produced MMP-9 promotes invasion *in vitro* and pulmonary metastasis in an orthotopic xenograft model of basal-like TNBC [25]. These observations suggest that MMP-3 is not merely a passive marker of tumor progression, but rather an active contributor to the invasive phenotype, making it an attractive candidate for therapeutic intervention.

Although MMPs have long been considered promising targets for cancer therapy, efforts to translate MMP inhibitors into the clinic have historically met with limited success [26]. Early generations of small-molecule MMP inhibitors were designed to broadly target the catalytic activity of multiple family members, but these agents frequently failed in clinical trials because of insufficient selectivity, dose-limiting toxicities, and the complex context-dependent roles of individual MMPs in tumor biology [27,28]. Broad-spectrum inhibition can disrupt not only tumor-promoting proteases but also MMPs with homeostatic or even protective functions, thereby limiting therapeutic benefit [29]. These failures underscored a critical lesson for the field, namely that successful therapeutic targeting of MMPs is likely to require highly selective approaches that discriminate among closely related proteases and preserve beneficial proteolytic functions while blocking disease-promoting activity [30,31,32]. Thus, rather than abandoning MMPs as targets altogether, current strategies increasingly emphasize precision targeting of individual proteases with defined pathological roles.

Nanobodies (VHH) offer a compelling platform for achieving this level of selectivity [33,34]. Derived from the variable domains of heavy-chain-only antibodies, nanobodies are small, stable, and highly engineerable binding molecules that can recognize epitopes that may be less accessible to conventional antibodies or difficult to target with small molecules [35,36]. Their compact size, robust biophysical properties, and capacity for high specificity make them attractive tools for both therapeutic development and mechanistic studies [37]. In the context of protease targeting, nanobodies may provide important advantages by enabling selective recognition of structural features unique to a given enzyme, as demonstrated by the identification of selective binders for individual MMPs using nanobodies and related antibody scaffolds [38,39,40]. As a result, nanobody-based inhibitors represent a promising strategy for revisiting protease targeting in cancer through a more precise and biologically informed framework [41].

Given the known contribution of MMP-driven proteolysis to tumor invasion and the longstanding challenge of achieving selective MMP inhibition, targeting MMP-3 with a nanobody may represent a novel approach for limiting invasive behavior in TNBC. By combining biochemical assessment of enzymatic inhibition with functional evaluation in cancer cell invasion models, such an approach can help determine whether targeting of MMP-3 translates into biologically meaningful anti-invasive effects.

In the present study, we employed a synthetic nanobody library to identify nanobody candidates targeting MMP-3 and assessed their inhibitory activity using an enzymatic kinetic assay with a fluorogenic substrate. To further determine whether MMP-3 contributes functionally to the invasive phenotype in MDA-MB-436 cells, we performed knockdown experiments and evaluated the effect of reduced *MMP3* expression on tumor cell invasion. We then tested whether nanobody-mediated inhibition of MMP-3 could suppress invasion in transwell invasion assays in a TNBC model. Collectively, these experiments were designed to establish MMP-3 as a functionally relevant driver of invasion and to evaluate nanobody-based inhibition as a feasible strategy to block this phenotype.

2. Materials and Methods

2.1 Cell Culture

TNBC cell lines MDA-MB-231(ATCC, HTB-26), BT-549 (ATCC, HTB-122), HCC1937 (ATCC, CRL-2336), MDA-MB-436 (ATCC, HTB-130), as well as SUM159 and SUM149 (both generous gift from Dr. Stephen P. Ethier, Medical University of South Carolina), were propagated from laboratory seed stocks and distribution stocks. Cell line identity was validated by short tandem repeat (STR) genotyping using the PowerPlex® 16 HS System (Promega) and tested negative for mycoplasma. MDA-MB-231 cells were maintained in Dulbecco's modified Eagle's medium (DMEM) supplemented with 10% fetal bovine serum (FBS). HCC1937 and BT-549 cells were maintained in RPMI 1640 supplemented with 10% FBS

and 0.023 IU/mL insulin. MDA-MB-436, SUM159, and SUM149 cells were maintained in DMEM/F12 supplemented with 10% FBS and 2.5 µg/mL insulin. All cell lines were cultured at 37 °C in a humidified atmosphere containing 5% CO_2 and were routinely monitored for appropriate morphology and growth characteristics.

2.2 Nanobody Library

A previously established synthetic nanobody yeast display library was utilized for nanobody selection, as described by McMahon and colleagues [42]. The library was expressed in the protease-deficient *Saccharomyces cerevisiae* strain BJ5465 and employs a yeast surface display system in which nanobodies are covalently tethered to the cell wall via a glycosylphosphatidylinositol (GPI) anchor through a flexible linker, rather than the conventional Aga2p fusion. The nanobody repertoire is based on a consensus VHH framework with diversified complementarity-determining regions (CDRs), enabling high sequence diversity and efficient *in vitro* selection of antigen-specific binders. Yeast transformants were maintained in selective synthetic dropout medium lacking tryptophan (SD-Trp) supplemented with 2% (w/v) dextrose for growth, and nanobody expression was induced by transferring cells to galactose-containing induction medium (SG-Trp) supplemented with 2% (w/v) galactose, as previously described [43].

2.3 MMP Expression, Purification, and Biotinylation

The catalytic domain of proMMP-3 lacking the C-terminal hemopexin region (proMMP-3cd) was recombinantly expressed in *Escherichia coli* using a pET3a expression system [44]. Following expression, the protein was isolated from inclusion bodies under denaturing conditions using a buffer containing 8 M urea, 20 mM Tris-HCl (pH 8.6), 20 mM DTT, and 50 µM $ZnCl_2$. The denatured protein was subsequently purified by anion-exchange chromatography on a Q-Sepharose column equilibrated in the same buffer and eluted with a linear NaCl gradient up to 0.5 M. Fractions containing proMMP-3cd were pooled, adjusted to an absorbance of approximately 0.3 at 280 nm, and refolded through stepwise dialysis against a buffer composed of 50 mM Tris-HCl (pH 7.5), 10 mM $CaCl_2$, and 150 mM NaCl. The refolded zymogen was then activated by incubation with 1 mM 4-aminophenylmercuric acetate at 37 °C overnight. The concentration of active MMP-3cd was determined by titration against a reference TIMP-1 stock [44]. For downstream applications, the active MMP-3cd was biotinylated using an NHS-PEG4-biotin reagent (Thermo Fisher Scientific) at a 1:10 molar ratio (protein:biotin) for 30 min at room temperature. Excess biotin was removed using desalting spin columns, and the extent of labeling was evaluated using a 4′-hydroxyazobenzene-2-carboxylic acid (HABA) assay according to the manufacturer's instructions.

2.4 Library Screening and Flow Cytometry Analysis

For the first round of magnetic-activated cell sorting (MACS), approximately 1×10^{10} *Saccharomyces cerevisiae* cells displaying the synthetic nanobody library were subjected to selection against biotinylated MMP-3cd [45]. An initial negative selection step was performed by incubating the yeast library with 50 µL of streptavidin-coated magnetic beads (Invitrogen, Thermo Fisher Scientific, Waltham, MA, USA) at 4×10^5 beads/µL, corresponding to 2×10^7 total beads, to deplete nonspecific bead binders. The unbound yeast population was then incubated with 100 nM of biotinylated MMP-3cd pre-immobilized on streptavidin-coated magnetic beads at 4 °C with rotation for 2 h. Following incubation, bead-bound yeast cells were isolated using magnetic separation, extensively washed with ice-cold PBSA to remove non-binders, and subsequently resuspended in media for recovery and expansion prior to further rounds of selection.

Following magnetic enrichment, yeast cells displaying nanobodies were expanded in selective medium at 30 °C with shaking (250 rpm) for 16–20 h until reaching an OD_{600} of approximately 2–5. For fluorescence-activated cell sorting (FACS), at least 5×10^7 cells were used per round to maintain adequate library coverage. Cells were harvested by centrifugation (3000 ×g, 5 min, 4 °C) and resuspended in induction medium consisting of tryptophan dropout medium supplemented with 6.7 g/L yeast nitrogen base, 3.8 g/L –Trp dropout supplement, 20 g/L galactose, and 10 mL/L penicillin–streptomycin. Induction was carried out at 17 °C with shaking (250 rpm) for 18–24 h to promote nanobody surface expression. Induced cells were washed with ice-cold PBSA buffer (PBS containing 1% bovine serum albumin) and incubated with biotinylated MMP-3cd for 1 h at room temperature. Following antigen incubation, cells were labeled with a mouse anti-HA antibody (Invitrogen, Thermo Fisher Scientific, Waltham, MA, USA) (1:100 dilution) for 30 min on ice to assess nanobody expression, followed by staining with goat anti-mouse IgG–Alexa Fluor 488 (Invitrogen, Thermo Fisher Scientific, Waltham, MA, USA) and streptavidin–Alexa Fluor 647 (Invitrogen, Thermo Fisher Scientific, Waltham, MA, USA) (both at 1:100 dilution) for 30 min on ice. After washing, cells were resuspended in PBSA and analyzed or sorted by flow cytometry. Unstained yeast cells were included as negative controls to establish background fluorescence and guide flow cytometry gating. Nanobody surface expression was detected in the Alexa Fluor 488 channel using anti-HA labeling, whereas binding of biotinylated MMP-3cd was detected in the Alexa Fluor 647 channel using streptavidin–Alexa Fluor 647. Gates were established relative to the background fluorescence of the unstained yeast controls to identify populations exhibiting nanobody surface expression and MMP-3cd binding. The percentage of events within the indicated gated population was determined for each sample. For enrichment of high-affinity

binders, three rounds of FACS were performed using progressively decreasing concentrations of biotinylated MMP-3cd (250 nM, 100 nM, and 25 nM) using Bigfoot spectral cell sorter (Thermo Fisher Scientific, Waltham, MA, USA). Sorted populations recovered in media and cultured overnight at 30 °C prior to subsequent rounds of induction and selection.

For comparisons of individual nanobody clones, induced yeast cells were incubated with 100 nM biotinylated MMP-3cd for 1 h at room temperature and stained as described above. For the TIMP-1-C4 (a potent engineered inhibitor of MMP-3 [46]) competition experiment, 100 nM biotinylated MMP-3cd was preincubated with 200 nM TIMP-1-C4 for 1 h at room temperature and stained as described above. Control samples were treated with the same concentration of MMP-3cd in the absence of TIMP-1-C4. For concentration-dependent binding analysis, yeast-displayed NbM3-15 was incubated with biotinylated MMP-3cd over a concentration range of 0.001–200 nM for 1 h at room temperature. Background-subtracted MMP-3cd-binding signals were normalized to nanobody surface expression and plotted against the total MMP-3cd concentration. The data were fitted by nonlinear regression using a one-site specific-binding model in GraphPad Prism 11 to determine the apparent equilibrium dissociation constant. Data were collected for a minimum of 10,000 events per sample, and fluorescence signals were analyzed using FlowJo software v10.10.0 (BD Life Sciences, Ashland, OR, USA). Binding was quantified as the geometric mean fluorescence intensity (gMFI) of the MMP-3cd signal (Alexa Fluor 647), normalized to nanobody surface expression (Alexa Fluor 488, anti-HA). Experiments were performed in biological triplicates, and results are presented as mean ± standard deviation. Statistical significance was assessed using one-way ANOVA with appropriate post hoc testing.

2.5 DNA Sequencing

Plasmid DNA was extracted from individual yeast clones using a yeast miniprep kit according to the manufacturer's instructions (Zymo Research). The recovered plasmids were subsequently transformed into electrocompetent *Escherichia coli* cells. Plasmid DNA from bacterial cultures was then purified using a standard plasmid miniprep system (Promega). Purified samples were submitted for Sanger sequencing, and resulting sequences were analyzed using SnapGene software (GSL Biotech).

2.6 Nanobody Expression and Purification

Recombinant NbM3-15, expressed from the pET26b expression construct with a C-terminal His-tag, was transformed into *Escherichia coli* BL21 (DE3) cells and plated on LB agar supplemented with kanamycin, followed by overnight incubation [42]. A single colony was used to inoculate LB medium for overnight growth, which was subsequently used to seed 2 L of Terrific Broth (TB) supplemented with 4% glycerol and kanamycin at a ratio of 10 mL starter culture per liter. Cultures were grown at 37 °C until reaching an OD_{600} of 1.5–2.0 (approximately 4 h), after which the temperature was reduced to 17 °C and cultures were allowed to equilibrate for 1 h prior to induction with 200 µM IPTG for overnight expression. Cells were harvested by centrifugation. For lysis, cell pellets were resuspended in 50 mL SET buffer (200 mM Tris, pH 8.0, 500 mM sucrose, 500 µM EDTA) per liter of initial culture volume. Following complete resuspension, two volumes of cold H_2O, 5 mM $MgCl_2$, and benzonase nuclease (Sigma-Aldrich, St. Louis, MO, USA) were added, and the mixture was stirred at room temperature for 1 h. Lysates were clarified by centrifugation, and the resulting supernatant was supplemented with 100 mM NaCl and stirred at room temperature for an additional 15 min. The clarified supernatant was filtered through a glass microfiber filter and applied to Ni-NTA resin (Cytiva, Marlborough, MA, USA) pre-equilibrated with wash buffer using an automated fast protein liquid chromatography (FPLC) system (ÄKTA pure, Cytiva). The resin was washed sequentially with 10 column volumes (CV) of wash buffer 1 (20 mM HEPES, pH 7.5, 500 mM NaCl, 20 mM imidazole) and 10 CV of wash buffer 2 (20 mM HEPES, pH 7.5, 100 mM NaCl, 20 mM imidazole). Bound NbM3-15 was subsequently eluted with 10–20 CV of elution buffer containing 20 mM HEPES, pH 7.5, 100 mM NaCl, and 200 mM imidazole. Protein-containing fractions were pooled and concentrated using a 10-kDa molecular-weight-cutoff centrifugal concentrator (Amicon). The purified nanobody was subsequently buffer exchanged by overnight dialysis into 20 mM HEPES, pH 7.5, 150 mM NaCl, and 10% glycerol. Protein concentration was determined using absorbance at 280 nm using the calculated extinction coefficient, and protein purity was assessed by SDS-PAGE. Purified NbM3-15 was aliquoted and stored at –80 °C until further use.

2.7 MMP Inhibition Studies

To evaluate the time dependence of inhibition, recombinant MMP-3cd (1 nM) was incubated with NbM3-15 (40 nM) in TNCB buffer (50 mM Tris-HCl, pH 7.5, 100 mM NaCl, 5 mM $CaCl_2$, and 0.05% Brij) at 37 °C for 0, 15, 30, 45, 60, 90, 120, 150, or 180 min. At each preincubation time point, enzymatic activity was initiated by addition of the fluorogenic peptide substrate Mca-Pro-Leu-Gly-Leu-Dap(Dnp)-Ala-Arg-NH_2 (final concentration, 10 µM; AnaSpec, Inc.). Fluorescence was monitored at 1-min intervals using excitation and emission wavelengths of 340 and 400 nm, respectively. Initial reaction rates were determined from the linear portion of the fluorescence-versus-time curves and expressed as percent residual MMP-3cd activity relative to the activity measured at the 0-min preincubation time point. Based on the time-course experiment, a 2-h preincubation period was used for equilibrium inhibition measurements. Recombinant MMP-3cd (1 nM) was

preincubated with NbM3-15 over a concentration range of 0–80 nM (0, 3, 5, 10, 15, 20, 30, 40, 60, and 80 nM) in TNCB buffer at 37 °C for 2 h. Enzymatic reactions were initiated by addition of fluorogenic peptide substrate to a final concentration of 10 µM, and fluorescence was recorded at 1-min intervals using excitation and emission wavelengths of 340 and 400 nm, respectively. Initial velocities were calculated from the linear phase of substrate cleavage and plotted as a function of total NbM3-15 concentration. Equilibrium inhibition constants (K_i) were determined by nonlinear regression using the Morrison tight-binding inhibition model, accounting for total enzyme and inhibitor concentrations and correcting for substrate concentration using an experimentally determined K_m of 6.70 µM for MMP-3cd, as previously described [47]. Data were fitted using GraphPad Prism 11 (GraphPad Software, Boston, MA, USA). Reported values represent the mean ± standard deviation from three independent experiments.

2.8 RNA Isolation and Quantitative Real-Time PCR

Human triple-negative breast cancer cell lines MDA-MB-231, BT-549, HCC1937, MDA-MB-436, SUM159, and SUM149 were used for comparative analysis of *MMP3* expression. Cells were propagated from laboratory seed stocks and distribution stocks that were validated by short tandem repeat genotyping through Genetica DNA Laboratories, Burlington, NC. MDA-MB-231 cells were grown in Dulbecco's modified Eagle's media (DMEM) with 10% FBS. HCC1937 and BT-549 cells were grown in RPMI 1640 media supplemented with 10% FBS and 0.023 IU/mL insulin. MDA-MB-436, SUM159 and SUM149 cells were maintained in DMEM/F12 supplemented with 10% FBS and 2.5 µg/mL insulin. All cell lines were maintained at 37 °C in a humidified incubator containing 5% CO_2 and were routinely monitored for appropriate morphology and growth characteristics.

For gene expression analysis, total RNA was extracted from cultured cells using TRIzol reagent (Thermo Fisher Scientific) according to the manufacturer's instructions. Complementary DNA (cDNA) was synthesized from purified RNA using the High-Capacity cDNA Reverse Transcription Kit (Applied Biosystems) according to the manufacturer's protocol. Quantitative real-time PCR (qRT-PCR) was performed using TaqMan Gene Expression Assays (Applied Biosystems) on a QuantStudio 7 Flex Real-Time PCR System (Applied Biosystems). *MMP3* transcript levels were quantified using the human *MMP3* TaqMan assay Hs00968305_m1, with GAPDH (Hs99999905_m1) serving as the endogenous reference control. Reactions were performed according to the manufacturer's recommended cycling conditions. Data were analyzed using QuantStudio 7 Flex software version 1.7.2, and relative gene expression was calculated with GAPDH used for normalization. The software was used to calculate relative quantification (RQ) using the $2^{-\Delta\Delta Ct}$ method based on mean Ct values, with uncertainty propagated in ΔCt space; RQ values are plotted as instrument-derived mean RQ ± error. For the qRT-PCR comparison of *MMP3* expression between NT and *MMP3*-KD cells, statistical significance was assessed using an unpaired t test in GraphPad Prism 11 (GraphPad Software, Boston, MA, USA).

2.9 Lentiviral shRNA Knockdowns

Short hairpin RNA (shRNA) targeting human *MMP3*, NM_002422.x-1512s1c1 (*MMP3*-KD), was obtained from the MISSION TRC-Hs shRNA library (Sigma-Aldrich, St. Louis, MO, USA). A non-targeting shRNA sequence with no known homology to human genes was used as the negative control (NT). Lentiviral particles were generated in HEK293FT cells according to the manufacturer's recommended protocol, and virus-containing conditioned medium was collected for transduction. MDA-MB-436 cells were seeded at a density of 1×10^6 cells per 10-cm culture dish and allowed to adhere for 24 h. Cells were then exposed to 2 mL of lentiviral supernatant in complete DMEM/F12 medium supplemented with 10% fetal bovine serum, 2.5 µg/mL insulin, and 10 µg/mL polybrene. After 24 h of transduction, the virus-containing medium was removed and replaced with fresh complete medium containing 1 µg/mL puromycin. Cells were maintained under puromycin selection for 72 h, after which the pooled surviving cell populations were harvested. Knockdown efficiency was assessed by qRT-PCR, and the selected populations were subsequently used for Matrigel transwell invasion assays.

2.10 Matrigel Transwell Invasion Assays

Invasion assays followed a protocol like that we have described previously [47]. MDA-MB-436 cells were obtained from validated laboratory stocks, with cell line authentication confirmed by short tandem repeat (STR) profiling (Genetica DNA Laboratories, Burlington, NC, USA). Cells were maintained in Dulbecco's Modified Eagle Medium/Nutrient Mixture F-12 (DMEM/F12) supplemented with 10% FBS and 2.5 µg/mL insulin at 37 °C in a humidified incubator containing 5% CO_2. Cells were cultured to approximately 80% confluence and replated at 2×10^6 cells per 100-mm dish 24 h before the invasion assay. For invasion assays, 24-well transwell inserts with 8.0-µm-pore membranes were coated with 50 µg Matrigel basement membrane matrix (Corning, Corning, NY, USA) diluted in 100 µL serum-free DMEM/F12 and incubated at 37 °C for 4 h. Residual coating solution was removed immediately before cell seeding. On the day of the assay, 1×10^5 cells were resuspended in serum-free DMEM/F12 containing 0.1% bovine serum albumin (BSA) and added to the upper chamber. The lower chamber contained 750 µL of serum-free NIH/3T3-conditioned medium supplemented with 50 µg/mL ascorbic acid as a chemoattractant. Each experimental condition was evaluated in triplicate wells.

For assessment of the effect of *MMP3* knockdown on invasion, MDA-MB-436 cells previously transduced with either non-targeting shRNA (NT) or the *MMP3*-targeting shRNA (*MMP3*-KD) were harvested following puromycin selection and seeded into the upper chambers under identical assay conditions. No NbM3-15 was added in this experiment. NT and *MMP3*-KD cells were allowed to invade for 18 h at 37 °C and 5% CO_2. For assessment of NbM3-15-mediated inhibition of invasion, non-transduced MDA-MB-436 cells were seeded into the upper chambers in the presence of NbM3-15 at final concentrations of 0, 100, 200, or 400 nM. NbM3-15 was added directly to the cell suspension in the upper chamber at the beginning of the assay and remained present throughout the entire 18-h invasion period. The untreated control received no NbM3-15. Following incubation for 18 h at 37 °C and 5% CO_2, non-invading cells were removed from the upper surface of each membrane by gentle swabbing. Cells that had invaded through the Matrigel and reached the lower membrane surface were fixed with methanol and stained with crystal violet. Images of stained membranes were acquired under identical microscopy settings, and crystal-violet-positive invading cells were quantified using INFINITY ANALYZE 6.5 software (Lumenera Corporation, Ottawa, Ontario, Canada). Both the *MMP3* knockdown and NbM3-15 concentration-response invasion experiments were performed independently three times, with three technical replicate wells per condition in each independent experiment. For inferential statistical analysis, the three independently performed experiments were considered the biological replicates (n = 3), whereas replicate wells within each experiment were considered technical replicates. The data displayed are from one representative experiment, and similar results were obtained in all three independent experiments. Statistical analyses were performed using GraphPad Prism 11 (GraphPad Software, Boston, MA, USA). For the *MMP3* knockdown experiment, NT and *MMP3*-KD groups were compared using an unpaired t test. For the NbM3-15 concentration-response experiment, differences among treatment groups were analyzed using ordinary one-way ANOVA, with each NbM3-15 concentration compared with the untreated (0 nM) control. Statistical significance was assessed using the three independent biological experiments (n = 3).

3. Results

3.1 Identification of Nanobodies With Enhanced Binding to MMP-3

To identify nanobody ligands targeting MMP-3cd, we enriched a yeast surface-displayed library of synthetic nanobodies for binders against purified human MMP-3cd using magnetic cell sorting (MACS) (Fig. 1A). We subsequently performed a two-color fluorescence-activated cell sorting (FACS)-based selection to isolate nanobodies that specifically recognize the catalytic domain of target protein (Fig. 1B). Following three rounds of FACS, a clear population shift was observed, with the proportion of nanobody variants exhibiting strong binding to MMP-3cd within the sorting gate increased from 17.9% in the library population after MACS to 53.4% in the final round of FACS (Fig. 1C). These results demonstrate effective enrichment of nanobody variants exhibiting increased binding to MMP-3cd.

3.2 Isolation of Individual MMP-3cd-Binding Nanobody Clones

From the enriched population, 24 randomly selected clones were sequenced, revealing ten unique nanobody sequences. Alignment of these candidates demonstrated sequence diversity across the complementarity-determining regions (CDRs), with particularly pronounced variation in CDR3 (Fig. 2A). To investigate whether the selected nanobodies recognize an epitope overlapping the MMP-3 active-site region, competitive binding experiments were performed using TIMP-1-C4, a potent engineered inhibitor of MMP-3 [46]. Binding of each yeast-displayed nanobody to MMP-3cd was measured in the absence or presence of TIMP-1-C4 and normalized to nanobody surface expression. Addition of TIMP-1-C4 significantly reduced MMP-3cd binding for all ten nanobody candidates (Fig. 2B), indicating competition for sterically overlapping binding sites on the MMP-3 catalytic domain and supporting recognition of epitopes at or near the active-site region. Based on its strong MMP-3cd binding signal and competitive behavior in the TIMP-1-C4 assay, NbM3-15 was selected for further quantitative characterization. Binding of MMP-3cd to yeast-displayed NbM3-15 was evaluated over a range of antigen concentrations by flow cytometry. Representative plots at 0.1, 10, and 100 nM MMP-3cd showed a progressive concentration-dependent shift toward the high-binding/high-expression population as the MMP-3cd concentration increased (Fig. 3A). Quantitative analysis of the concentration-dependent binding data by nonlinear regression using a one-site binding model yielded an apparent equilibrium dissociation constant (K_d^{app}) of 1.26 nM for NbM3-15 (Fig. 3B). These results demonstrate that NbM3-15 binds MMP-3cd with low-nanomolar apparent affinity and support its selection as the lead nanobody for subsequent biochemical and functional characterization.

3.3 NbM3-15 Nanobody Demonstrates High MMP-3 Inhibition Potency

To extend our findings and quantitatively assess the protease-inhibitory activity of the NbM3-15 nanobody in solution, we cloned, expressed, and purified the soluble protein using an *E. coli* expression system. We then evaluated inhibition of MMP-3cd activity using a fluorometric enzyme assay that monitors reduced substrate cleavage in the presence of increasing concentrations of the nanobody (Fig. 4A). We next investigated the time dependence of NbM3-15-mediated MMP-3 inhibition. MMP-3cd (1 nM)

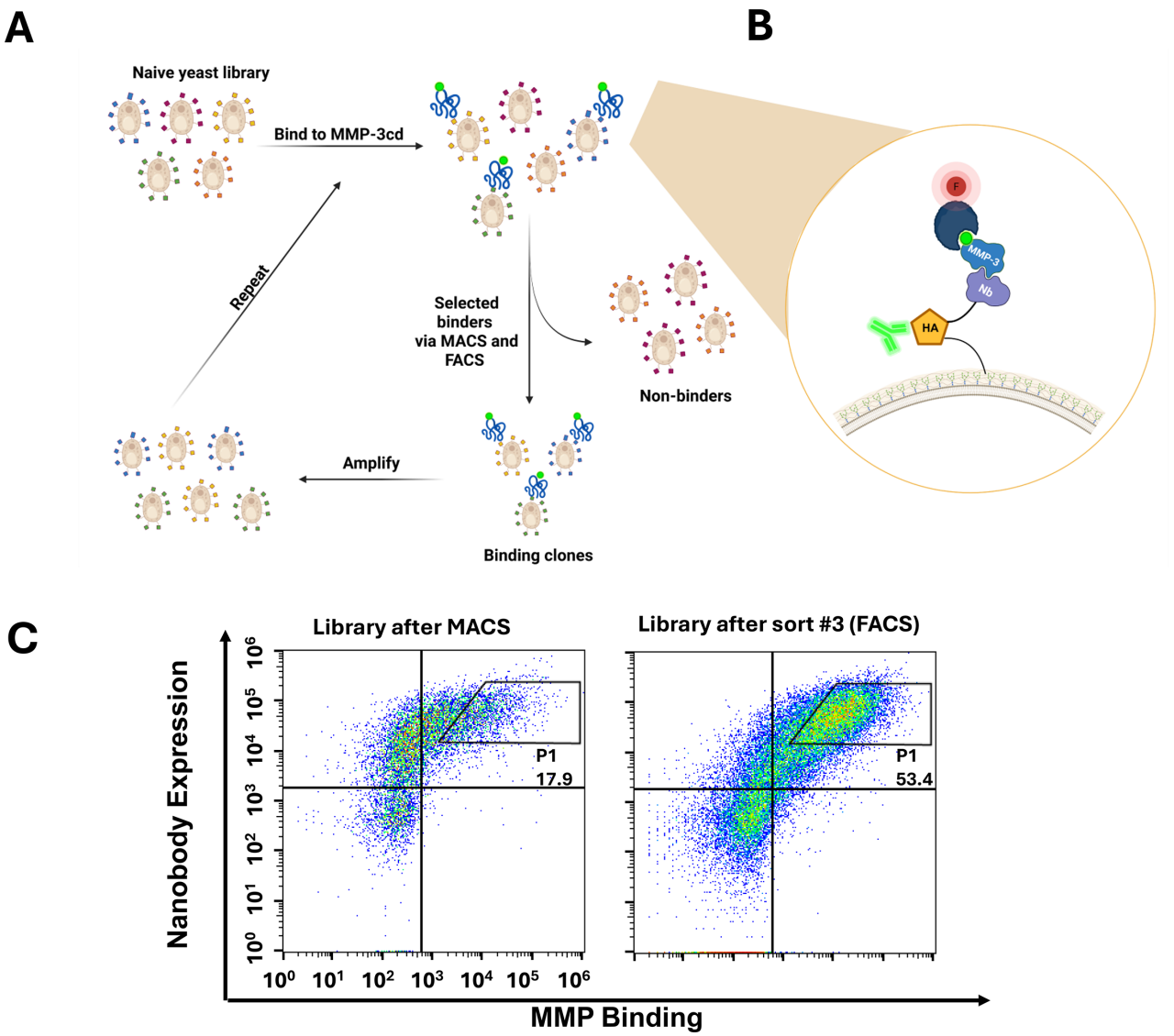


Fig. 1. Enrichment of MMP-3-binding nanobodies from a yeast surface display library. (A) Schematic overview of the nanobody selection workflow. A naïve yeast-displayed synthetic nanobody library was incubated with biotinylated MMP-3cd, and antigen-binding clones were enriched through magnetic-activated cell sorting (MACS), followed by iterative fluorescence-activated cell sorting (FACS) and amplification. (B) Two-color staining strategy used to evaluate nanobody surface expression and MMP-3 binding. Nanobody expression was detected through the HA tag, while MMP-3 binding was detected using fluorophore-conjugated streptavidin. (C) Representative flow cytometry plots showing enrichment of MMP-3-binding clones after MACS and after the third FACS sort. The gated binding population increased from 17.9% to 53.4%, indicating successful enrichment of MMP-3–reactive nanobody variants. *MMP3*, matrix metalloproteinase-3.

was incubated with NbM3-15 (40 nM) for increasing time intervals before addition of fluorogenic substrate. Enzymatic activity progressively decreased with longer incubation times, indicating time-dependent formation of the inhibitory nanobody-MMP-3 complex. Approximately 75% activity remained after 45 min of incubation, whereas only approximately 25% activity remained after 60 min. By 120 min, residual MMP-3 activity was nearly undetectable, indicating near-complete inhibition under these conditions (Fig. 4B). Based on these results, a 2 h preincubation period was used for the subsequent concentration-dependent inhibition assay to allow the MMP-3cd-NbM3-15 complex to approach equilibrium before measurement of initial reaction rates and determination of (K_i) by Morrison tight-binding analysis. Using this empirically defined 2 h preincubation period, NbM3-15 produced a concentration-dependent reduction in MMP-3cd activity (Fig. 4C). Fitting the inhibition data to Morrison's tight-binding equation yielded a (K_i) value of 1.64 ± 0.1 nM, demonstrating potent inhibition of MMP-3cd by NbM3-15. Notably, these

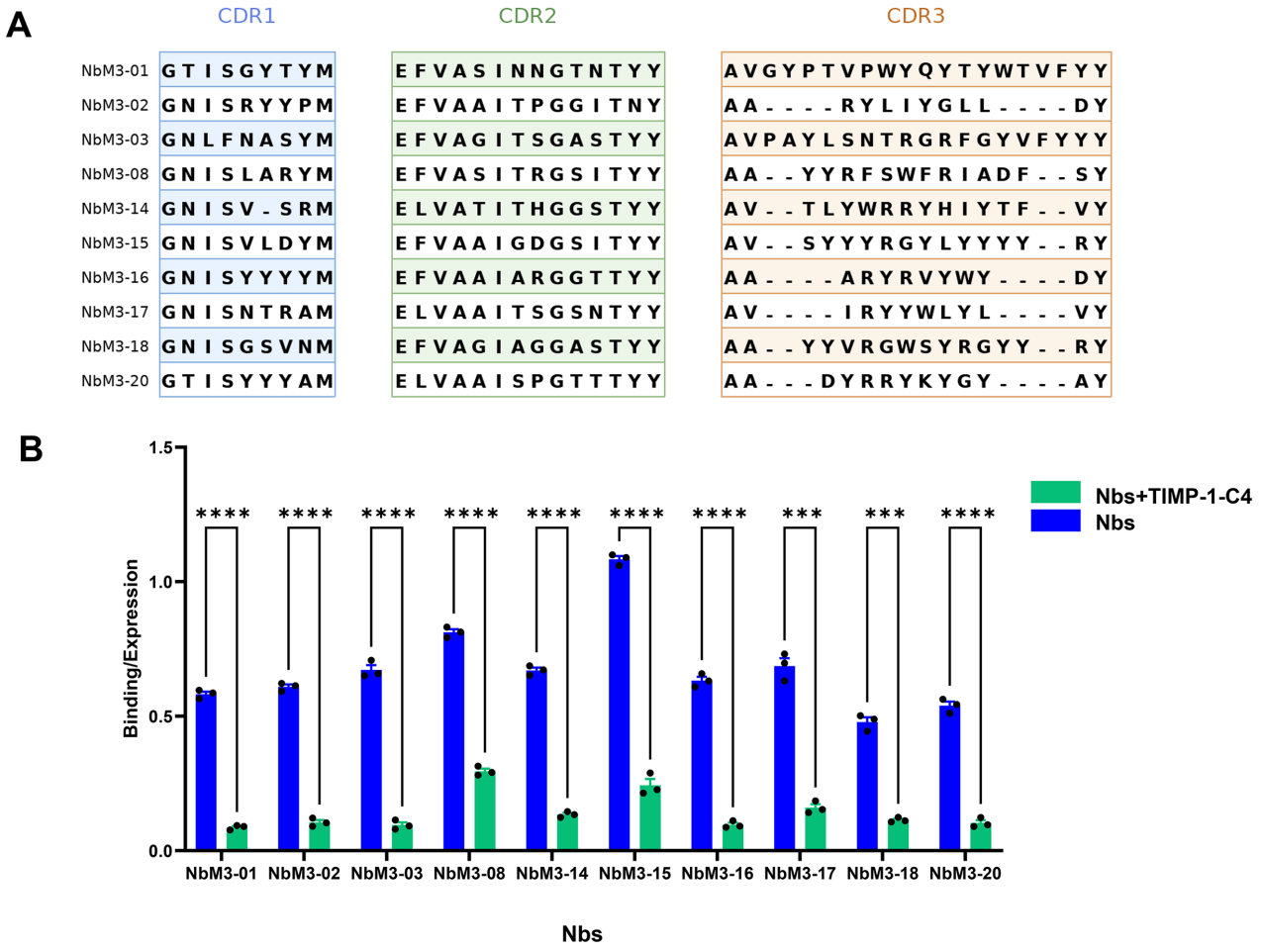


Fig. 2. Sequence analysis of selected MMP-3-binding nanobodies and competitive binding with TIMP-1-C4. (A) Alignment of the CDR1, CDR2, and CDR3 sequences of the ten unique nanobody clones identified following selection against MMP-3cd. (B) Competitive binding analysis of yeast-displayed nanobody candidates to 100 nM biotinylated MMP-3cd in the absence or presence of TIMP-1-C4. MMP-3cd binding was quantified as the ratio of the Alexa Fluor 647 binding signal to the Alexa Fluor 488 nanobody expression signal. Addition of TIMP-1-C4 significantly reduced MMP-3cd binding for all ten nanobody candidates, consistent with competition for sterically overlapping binding sites at or near the MMP-3 active-site region. Data are presented as mean ± SD from triplicate measurements. ***$p < 0.001$, ****$p < 0.0001$.

solution-based results were consistent with the yeast surface display findings, with NbM3-15 exhibiting inhibition potency in the low-nanomolar range. Together, these results provide converging evidence from both solution assays and YSD that this nanobody binds tightly to MMP-3cd and functions as a highly potent inhibitor.

3.4 MMP-3 Contributes to Invasion of Triple-Negative Breast Cancer Cells

To determine whether *MMP3* expression contributes to malignant progression in TNBC, we first assessed its expression across a panel of established TNBC cell lines. Among these, the MDA-MB-436 cell line exhibited markedly elevated *MMP3* transcript levels compared to all other lines examined (Fig. 5A), identifying it as a suitable model for invasion assays. To investigate the functional role of MMP-3, MDA-MB-436 cells were stably transduced with either a non-targeting (NT) control vector or a lentiviral shRNA construct targeting *MMP3*. Efficient knockdown was confirmed by qRT-PCR (Fig. 5B). Functional assessment using Matrigel transwell invasion assays revealed that *MMP3* gene silencing significantly reduced the invasive capacity of MDA-MB-436 cells (Fig. 5C), supporting a role for MMP-3 in promoting tumor cell invasion.

3.5 Dose-Dependent Inhibition of TNBC Cell Invasion by the NbM3-15 Nanobody

To determine whether the affinity of NbM3-15 toward MMP-3 translates into suppression of cancer cell invasion, Matrigel invasion assays were performed using MDA-MB-436 cells. Cells were treated with increasing concentrations (100–400 nM) of NbM3-15, and invading cells were quan-

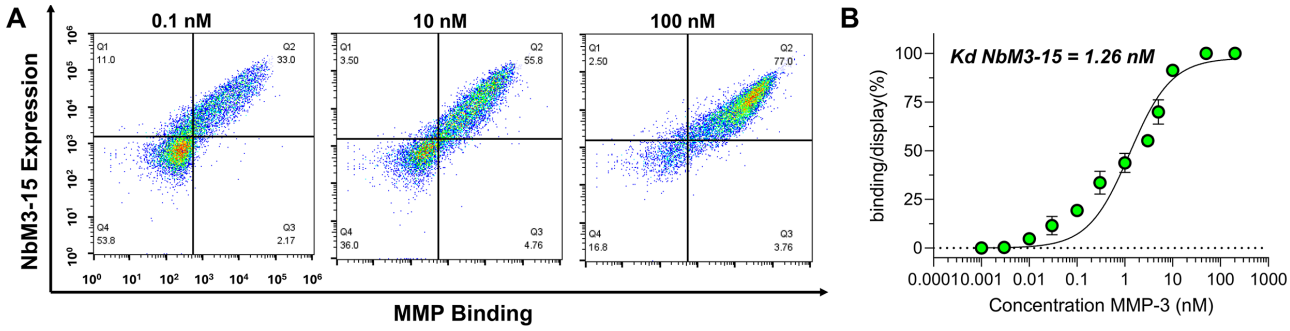


Fig. 3. Concentration-dependent binding of NbM3-15 to MMP-3cd. (A) Representative flow cytometry plots showing concentration-dependent binding of biotinylated MMP-3cd to yeast-displayed NbM3-15 at 0.1, 10, and 100 nM MMP-3cd. The horizontal and vertical gates were established relative to unstained yeast controls and distinguish nanobody expression-positive versus expression-negative events and MMP-3cd binding-positive versus binding-negative events, respectively. The upper-right quadrant represents yeast cells positive for both NbM3-15 surface expression and MMP-3cd binding; the percentages shown in each quadrant indicate the proportion of displayed events falling within the corresponding expression/binding population. Increasing MMP-3cd concentrations produced a progressive shift toward the high-binding/high-expression population. (B) Concentration-dependent binding of MMP-3cd to yeast-displayed NbM3-15. Binding signals were normalized to nanobody surface expression and analyzed by nonlinear regression using a one-site binding model, yielding an apparent dissociation constant (K_d^{app}) of 1.26 nM. Data are presented as mean ± SD from biological triplicates.

tified (Fig. 6). Treatment with nanobody inhibitor led to a clear, dose-dependent reduction in invasion, confirming functional activity. One-way ANOVA demonstrated highly significant effects of NbM3-15 concentration, indicating strong dose-dependent inhibition.

4. Discussion

In this study, we identified NbM3-15 as a potent MMP-3-targeting nanobody and illustrated how MMP-3 contributes functionally to invasion in an *MMP3*-high TNBC model. The complementary effects of *MMP3* knockdown and NbM3-15-mediated inhibition support the feasibility of targeting MMP-3 to suppress the invasive phenotype.

MMPs contribute to cancer progression by remodeling the extracellular matrix and regulating processes that promote invasion and metastasis [48]. MMP-3 additionally activates other proteases, amplifying proteolytic pathways that can promote malignant progression [49]. Prior work has linked MMP-3 to epithelial transformation, invasion, and tumor progression, and our findings are consistent with that broader view [16,20]. The reduction in invasion observed following shRNA-mediated *MMP3* knockdown supports a functional contribution of MMP-3 to invasion in this TNBC model.

The present findings are also relevant to efforts to overcome the historical limitations of broad-spectrum MMP inhibitors, particularly insufficient selectivity and off-target effects [50]. That lack of precision led to off-target effects and toxicities, while also interfering with MMPs that may play homeostatic or even protective roles [28]. Protein-based inhibitors offer an alternative strategy by exploiting larger interaction surfaces that may enable discrimination among closely related MMP family members [51,52]. Within this framework, display-based protein engineering platforms provide an especially valuable opportunity for the development of selective protease inhibitors [53]. Such approaches allow high-throughput screening of large libraries while preserving proper folding and functional presentation of complex protein scaffolds [54]. Tissue Inhibitors of Metalloproteinases (TIMP) engineering studies showed that simultaneous diversification of both N- and C-terminal interaction surfaces could improve MMP recognition and reveal earlier underappreciated domain cooperativity [44,47,51]. In the case of MMPs, where catalytic domains are highly conserved, such features are especially important because meaningful selectivity likely depends on recognizing fine structural features near the active site or at surrounding surfaces that contribute to substrate recognition and inhibitor binding. Our competition data suggest that the selected nanobodies engage the active-site region of MMP-3, and the strong inhibitory potency of NbM3-15 indicates that this recognition is functionally relevant; additional studies will be needed to define the selectivity profile of NbM3-15.

The broader literature also supports the feasibility of developing antibody-derived binders such as nanobodies or scFvs against proteases with both high selectivity and meaningful biological activity. Beyond metalloproteinases, nanobody engineering has yielded highly selective inhibitors of other cancer-associated proteases, including trypsin-3, demonstrating that this scaffold can overcome the selectivity challenges common to closely related protease families [41]. Within the metalloproteinase field, nanobody-based or related single-domain strategies have already been described for several targets. For MMP-2,

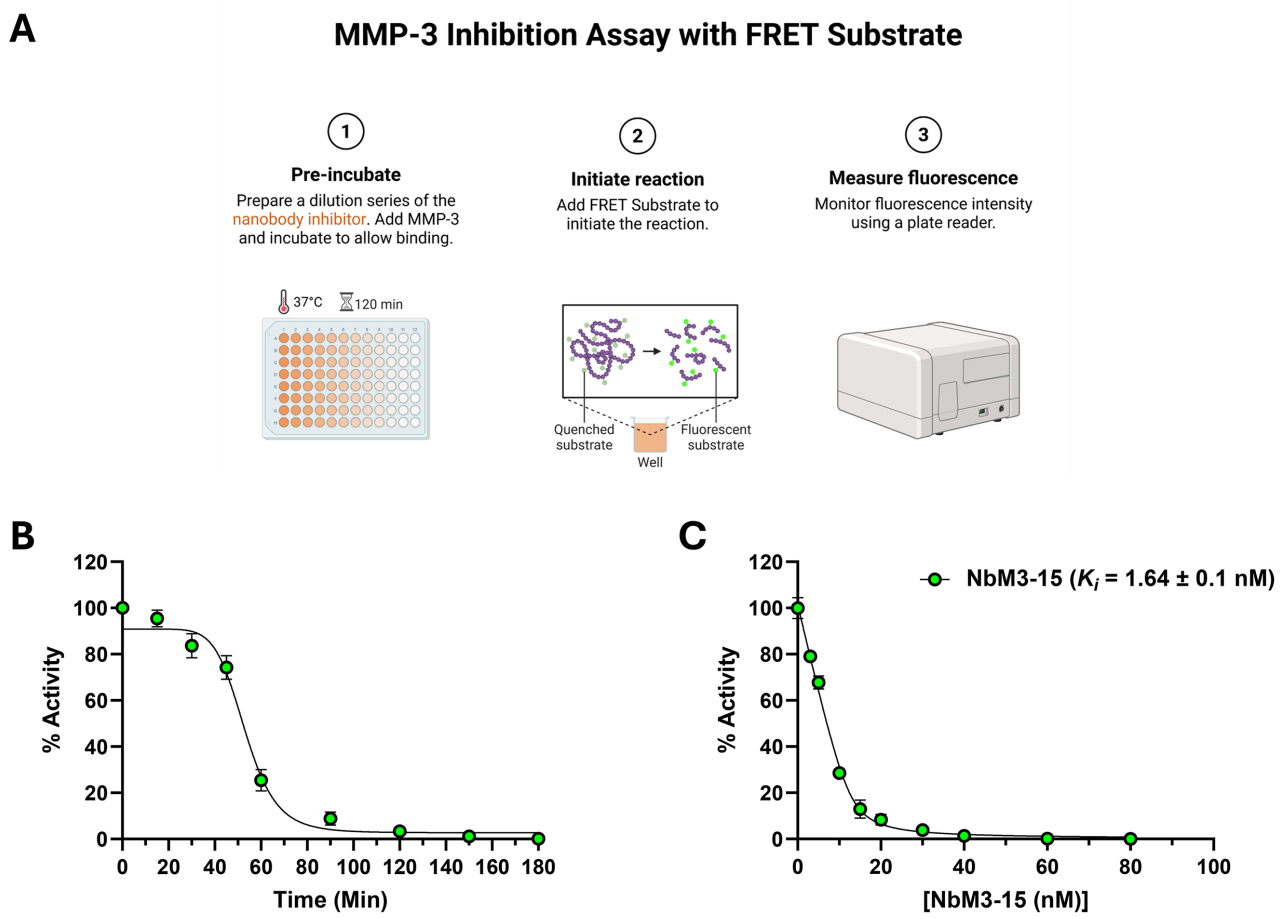


Fig. 4. Soluble NbM3-15 potently inhibits MMP-3 enzymatic activity. (A) Schematic of the fluorescence-based MMP-3 inhibition assay. MMP-3 was preincubated with serial dilutions of NbM3-15, the FRET substrate was added to initiate the reaction, and fluorescence was monitored over time using a plate reader. (B) Time-dependent inhibition of MMP-3 (1 nM) by NbM3-15 (40 nM), showing progressive reduction of enzymatic activity and near-complete inhibition by approximately 120 min. (C) Dose-response inhibition curve showing reduced MMP-3 activity with increasing concentrations of NbM3-15. Fitting to the Morrison tight-binding inhibition model yielded a K_i of 1.64 ± 0.1 nM. Data are presented as mean ± SD from three independent experiments (n = 3).

inhibitory and noninhibitory nanobodies were developed as potential therapeutic and diagnostic tools [40], whereas MMP-14-targeting nanobodies were generated as TNBC-directed imaging probes [55]. Single-domain antibody approaches have also achieved selective active-site-directed inhibition of MMP-10 [39], and nanobody-based inhibition has been reported for MMP-8, providing proof of principle that small antibody fragments can directly interfere with metalloproteinase activity [56]. In parallel, synthetic antibody engineering and yeast surface display approaches have been successfully applied to additional metalloproteinase family members, including selective active-site-directed binders against MMP-14 [38] and engineered scFv variants targeting ADAM-17 [57], further underscoring the adaptability of compact antibody scaffolds for selective metalloproteinase recognition. Together, these studies show that antibody-derived small binding scaffolds can provide the affinity, selectivity, and functional versatility needed to revisit protease targeting in cancer and related diseases. To the best of our knowledge, however, the present study is the first to report an MMP-3-targeting nanobody that demonstrates functional activity in both biochemical inhibition assays and cell-based invasion models.

A notable strength of the present study is the convergence of biochemical and functional evidence. Screening and binding analyses identified nanobody candidates with strong interaction with MMP-3, and soluble expression of NbM3-15 confirmed that this translated into potent inhibition in solution. Importantly, these enzymatic findings were directly linked to biological consequences through invasion assays in a relevant TNBC model. This is a critical point, because inhibition of purified protease activity does not always predict functional activity in cell-based systems [58,59,60], where localization, substrate availability, microenvironmental context, and interactions with endogenous regulators can all shape outcomes. Here, the combina-

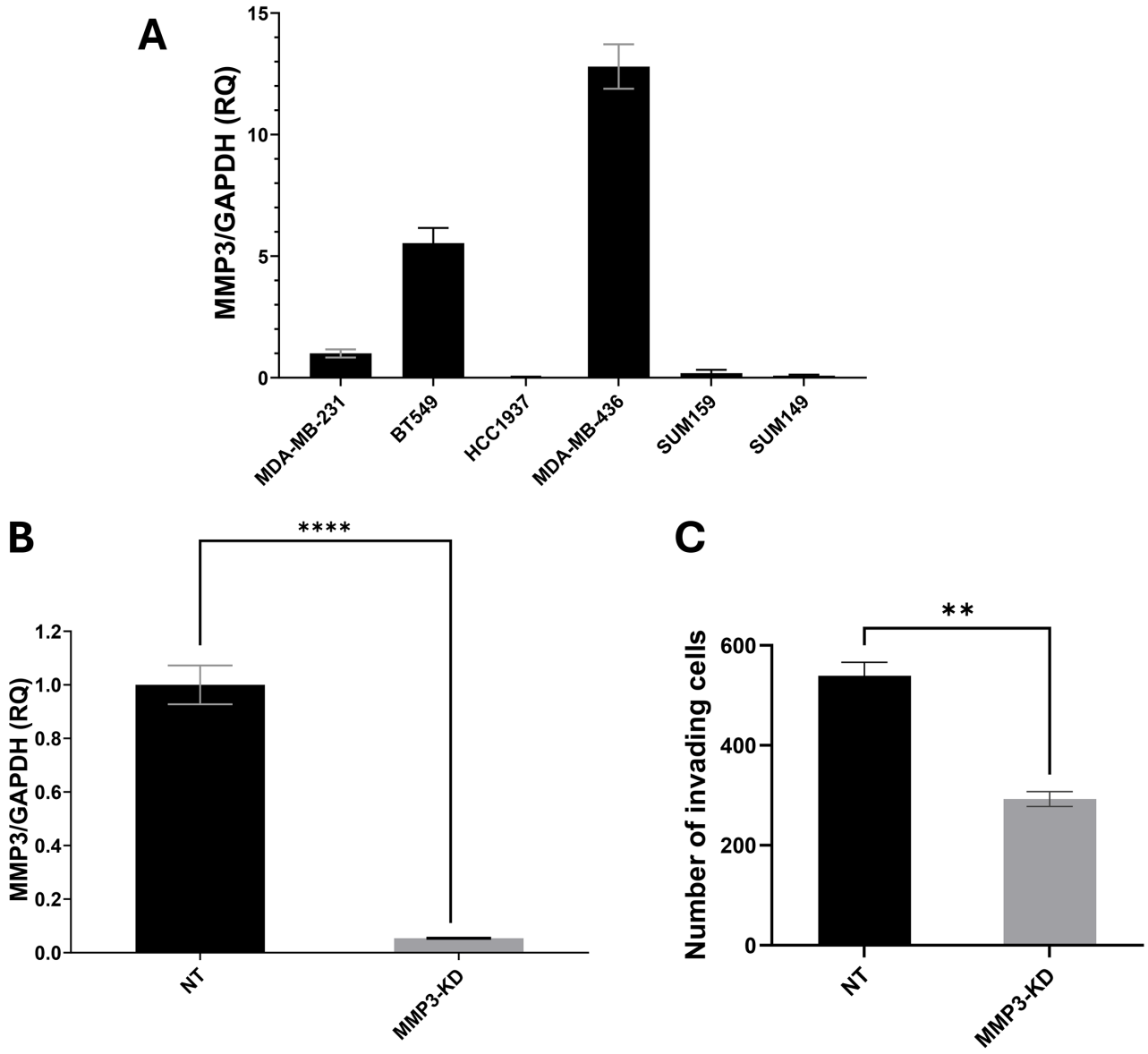


Fig. 5. *MMP3* knockdown suppresses invasion of MDA-MB-436 triple-negative breast cancer cells. (A) qRT-PCR analysis of *MMP3* expression across a panel of triple-negative breast cancer cell lines, identifying MDA-MB-436 cells as a high-*MMP3*-expressing model. This analysis was performed as a descriptive screen to identify an *MMP3*-high cell line for subsequent functional studies; no statistical comparisons between cell lines were performed. (B) qRT-PCR confirmation of *MMP3* knockdown in MDA-MB-436 cells transduced with an shRNA construct targeting *MMP3* compared with non-targeting control cells; error bars represent the instrument-derived RQ error from technical replicate reactions. (C) Matrigel transwell invasion assay showing that *MMP3* knockdown significantly reduced the invasive capacity of MDA-MB-436 cells. Data shown are from one representative experiment and are presented as mean ± SD of three technical replicate wells. The invasion experiment was independently performed three times with similar results. Statistical analysis was based on three independent biological experiments (n = 3). (**, $p < 0.01$; ****, $p < 0.0001$).

tion of elevated *MMP3* expression in MDA-MB-436 cells, reduced invasion following *MMP3* knockdown, and dose-dependent suppression of invasion by NbM3-15 provides complementary genetic and pharmacological evidence consistent with a functional contribution of MMP-3 to the observed anti-invasive phenotype.

The identification of MDA-MB-436 cells as a relatively *MMP3*-high TNBC model was also important for the study design. TNBC is molecularly heterogeneous, and dependence on individual proteases is unlikely to be uniform across models. By first surveying expression across a panel of TNBC cell lines and then selecting a model with elevated *MMP3* expression, we were better positioned to evaluate whether this protease represents a functional vulnerability. The knockdown experiments strengthened this interpretation by providing orthogonal genetic evidence that MMP-3

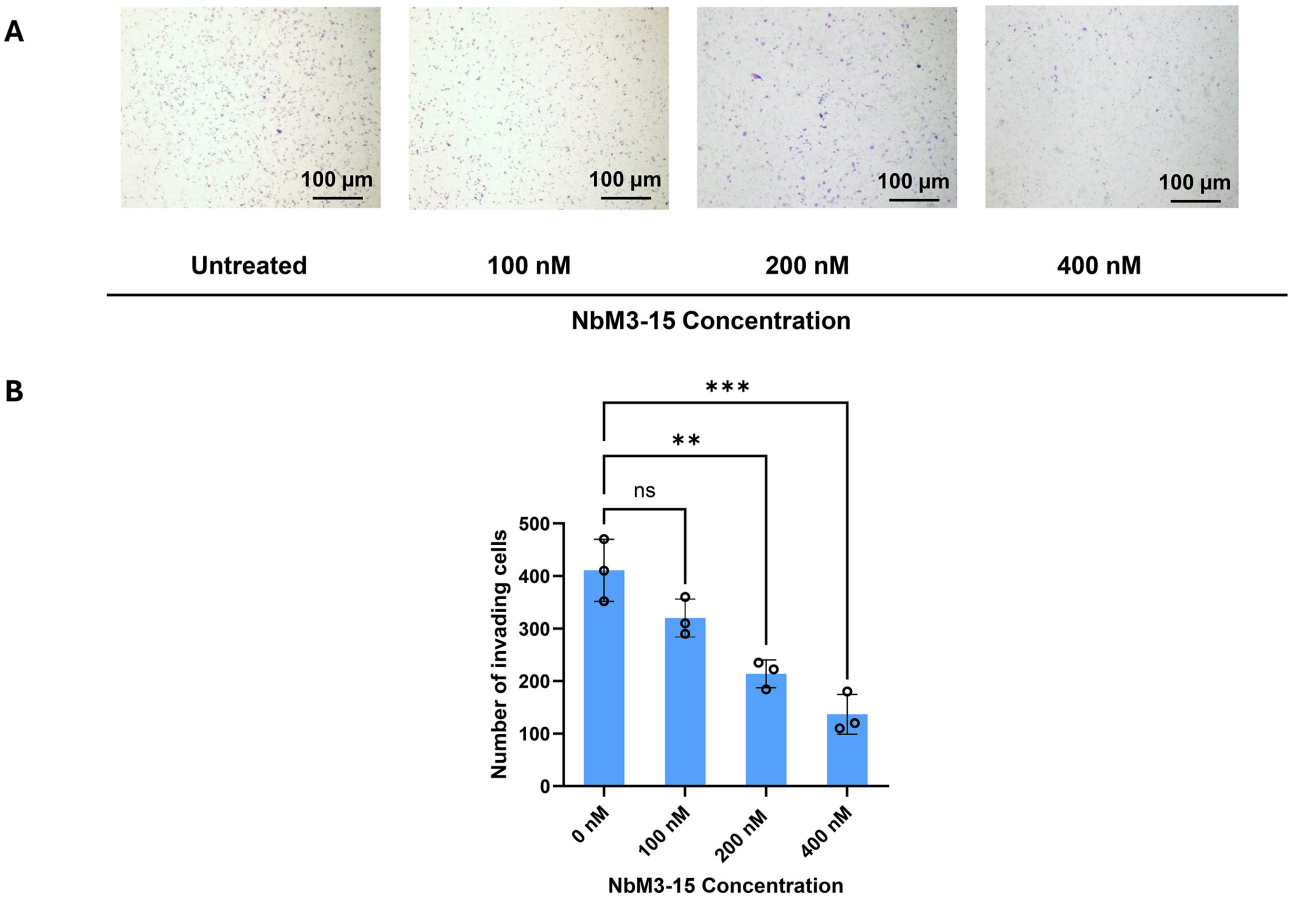


Fig. 6. NbM3-15 suppresses MDA-MB-436 cell invasion in a dose-dependent manner. (A) Representative images of crystal violet–stained MDA-MB-436 cells that invaded through Matrigel-coated transwell membranes following treatment with 0 (untreated), 100, 200, or 400 nM NbM3-15. Scale bars = 100 µm. (B) Quantification of invading cells following treatment with the indicated concentrations of NbM3-15. NbM3-15 reduced invasion in a dose-dependent manner, with significant inhibition at 200 and 400 nM compared with the untreated control. Treatment with 100 nM NbM3-15 reduced invasion but did not reach statistical significance. Data shown are from one representative experiment and are presented as mean ± SD of three technical replicate wells. The invasion experiment was independently performed three times with similar results. Statistical analysis was based on three independent biological experiments (n = 3). ns, not significant; $^{**}p < 0.01$; $^{***}p < 0.001$.

contributes to the invasive phenotype. Thus, the nanobody inhibition data do not stand alone, but are supported by a corresponding loss-of-function genetic framework.

Importantly, *MMP3* expression across TNBC cell lines should not be interpreted as a direct predictor of invasive capacity. Tumor invasion is multifactorial, and different TNBC models may rely on distinct proteolytic and non-proteolytic mechanisms. Thus, highly invasive cells with lower *MMP3* expression, such as MDA-MB-231, may depend on MMP-3-independent pathways [61,62]. Our expression survey was used to identify an *MMP3*-high model for functional evaluation, rather than to establish a correlation between *MMP3* expression and invasiveness. Accordingly, our findings demonstrate a functional contribution of MMP-3 to invasion in MDA-MB-436 cells, while studies across additional TNBC models will help define the broader relevance of MMP-3 targeting.

Another important next step will be structural characterization of the nanobody-MMP-3 complex. Although competition studies suggest active-site region engagement, the precise molecular determinants of binding remain unknown. High-resolution structural approaches, including X-ray crystallography, could reveal whether NbM3-15 contacts residues directly within the catalytic cleft, engages adjacent loops or exosites, or stabilizes a conformation that limits substrate access. Such information would be valuable not only for mechanistic understanding, but also for future optimization of affinity, specificity, and biophysical properties. Given previous studies [47,63,64] showing that variable exosite interactions and cooperative effects between spatially separated residues can contribute to TIMP-MMP recognition and selectivity, structural analysis may similarly reveal whether the MMP-3 nanobody exploits distinctive surfaces beyond the conserved catalytic core.

From a translational perspective, the anti-invasive activity of NbM3-15 suggests that NbM3-15-mediated MMP-3 inhibition may contribute to strategies aimed at limiting tumor dissemination in TNBC. In a disease setting where targeted options remain limited and metastatic progression remains a major clinical challenge, approaches that interfere with invasion are of considerable interest. Whether an MMP-3 nanobody would ultimately function best as a direct therapeutic, as part of a multispecific construct, or as a targeting component within a larger delivery platform remains to be determined. Nonetheless, the current findings establish proof of principle that nanobody-mediated inhibition of MMP-3 can generate a measurable functional effect in a biologically relevant cancer model. Recent advances in precision-targeted therapies and immunotherapeutic strategies further highlight the growing emphasis on identifying actionable molecular vulnerabilities to improve treatment options for TNBC [65].

5. Limitations

Some limitations should be considered. First, the invasion assays were conducted using a simplified *in vitro* Matrigel transwell system that cannot fully recapitulate the structural and cellular complexity of the tumor microenvironment. Although *MMP3* knockdown significantly reduced invasion, the effect was only partial, suggesting that invasion of MDA-MB-436 cells is not exclusively dependent on MMP-3 and may involve additional proteases or other invasion-promoting pathways. Notably, treatment with 400 nM NbM3-15 resulted in a greater reduction in invasion than that observed following *MMP3* knockdown. However, these effects cannot be directly compared because the degree of functional MMP-3 suppression achieved by genetic knockdown and nanobody-mediated inhibition may differ. *In vivo*, MMP-3 activity is likely shaped by stromal interactions, extracellular matrix organization, cytokine signaling, and cooperation with other proteases. Accordingly, studies in more physiologically relevant models, including 3D culture systems, organoid-based platforms, and *in vivo* xenografts, will be important for establishing the therapeutic relevance of NbM3-15.

Second, functional evaluation was focused on the *MMP3*-high MDA-MB-436 model, supporting further investigation of MMP-3 targeting in TNBC but limiting the generalizability of the present findings. Evaluation across additional TNBC models with varying levels of *MMP3* expression will help determine the broader applicability of this approach and identify biological contexts in which MMP-3 inhibition may be most effective. In addition, the cellular effects of NbM3-15 were assessed using Matrigel transwell invasion assays; complementary measurements of cell viability, proliferation, and Matrigel-independent migration will help distinguish the cellular processes contributing to the observed anti-invasive activity. Finally, broader selectivity profiling against closely related and invasion-associated metalloproteinases, including MMP-10, MMP-2, and MMP-9, will be important. Because the translational potential of NbM3-15 depends not only on its potency but also on its specificity, systematic assessment of cross-reactivity will be necessary to establish how selectively it distinguishes MMP-3 from other family members and to guide its further development.

6. Conclusions

We identified NbM3-15 as a potent nanobody inhibitor of MMP-3 and showed that targeting MMP-3 suppresses invasion in an *MMP3*-high TNBC model. These findings provide proof of principle for nanobody-mediated inhibition of MMP-3 and support further characterization of NbM3-15, including MMP-family selectivity profiling, structural analysis, and evaluation in additional biological models. More broadly, this study adds to growing evidence that modern protein engineering platforms can revive protease targeting through approaches that emphasize specificity, mechanistic precision, and biologically meaningful functional validation.

Availability of Data and Materials

All original contributions presented in this study are included in the article. Any further inquiries should be directed to the corresponding author.

Author Contributions

Conceptualization, AS, DCR and ESR; methodology, AMD, AS, AH and MAC; validation, AMD, AS, AH; formal analysis, AS, DCR and ESR; investigation, AMD, AS, AH and MAC; resources, AS, ESR, and DCR; writing—original draft preparation, AMD and AS; writing—review and editing, AS, DCR and ESR; visualization, MAC; supervision, AS. All authors have read and agreed to the published version of the manuscript. All authors contributed to editorial changes in the manuscript. All authors have participated sufficiently in the work and agreed to be accountable for all aspects of the work.

Ethics Approval and Consent to Participate

Not applicable.

Acknowledgment

Not applicable.

Funding

This research received no external funding.

Conflicts of Interest

The authors declare no conflicts of interest.

References

[1] Dessie ZG, Zewotir T. Global determinants of breast cancer mortality: a comprehensive meta-analysis of clinical, demographic, and lifestyle risk factors. BMC Public Health. 2025; 25: 2640. https://doi.org/10.1186/s12889-025-24036-w

[2] Carvalho E, Canberk S, Schmitt F, Vale N. Molecular Subtypes and Mechanisms of Breast Cancer: Precision Medicine Approaches for Targeted Therapies. Cancers. 2025; 17: 1102. https://doi.org/10.3390/cancers17071102

[3] Aysola K, Desai A, Welch C, Xu J, Qin Y, Reddy V, et al. Triple Negative Breast Cancer - An Overview. Hereditary Genetics: Current Research. 2013; 2013: 001. https://doi.org/10.4172/2161-1041.S2-001

[4] Bianchini G, Balko JM, Mayer IA, Sanders ME, Gianni L. Triple-negative breast cancer: challenges and opportunities of a heterogeneous disease. Nature Reviews. Clinical Oncology. 2016; 13: 674–690. https://doi.org/10.1038/nrclinonc.2016.66

[5] Newton EE, Mueller LE, Treadwell SM, Morris CA, Machado HL. Molecular Targets of Triple-Negative Breast Cancer: Where Do We Stand? Cancers. 2022; 14: 482. https://doi.org/10.3390/cancers14030482

[6] Pauli BU, Schwartz DE, Thonar EJ, Kuettner KE. Tumor invasion and host extracellular matrix. Cancer Metastasis Reviews. 1983; 2: 129–152. https://doi.org/10.1007/BF00048966

[7] Chang J, Chaudhuri O. Beyond proteases: Basement membrane mechanics and cancer invasion. The Journal of Cell Biology. 2019; 218: 2456–2469. https://doi.org/10.1083/jcb.201903066

[8] Kessenbrock K, Plaks V, Werb Z. Matrix metalloproteinases: regulators of the tumor microenvironment. Cell. 2010; 141: 52–67. https://doi.org/10.1016/j.cell.2010.03.015

[9] Niland S, Riscanevo AX, Eble JA. Matrix Metalloproteinases Shape the Tumor Microenvironment in Cancer Progression. International Journal of Molecular Sciences. 2021; 23: 146. https://doi.org/10.3390/ijms23010146

[10] Fingleton B. Matrix metalloproteinases: roles in cancer and metastasis. Frontiers in Bioscience: a Journal and Virtual Library. 2006; 11: 479–491. https://doi.org/10.2741/1811

[11] Curran S, Murray GI. Matrix metalloproteinases: molecular aspects of their roles in tumour invasion and metastasis. European Journal of Cancer (Oxford, England: 1990). 2000; 36: 1621–1630. https://doi.org/10.1016/s0959-8049(00)00156-8

[12] Duffy MJ, Maguire TM, Hill A, McDermott E, O'Higgins N. Metalloproteinases: role in breast carcinogenesis, invasion and metastasis. Breast Cancer Research. 2000; 2: 252–257. https://doi.org/10.1186/bcr65

[13] Egeblad M, Werb Z. New functions for the matrix metalloproteinases in cancer progression. Nature Reviews Cancer. 2002; 2: 161–174. https://doi.org/10.1038/nrc745

[14] Wan J, Zhang G, Li X, Qiu X, Ouyang J, Dai J, et al. Matrix Metalloproteinase 3: A Promoting and Destabilizing Factor in the Pathogenesis of Disease and Cell Differentiation. Frontiers in Physiology. 2021; 12: 663978. https://doi.org/10.3389/fphys.2021.663978

[15] Jiang J, Wu Q, Rajasekaran S, Wu R. MMP3 at the crossroads: Linking molecular pathways to disease diagnosis and therapy. Pharmacological Research. 2025; 216: 107750. https://doi.org/10.1016/j.phrs.2025.107750

[16] Sternlicht MD, Lochter A, Sympson CJ, Huey B, Rougier JP, Gray JW, et al. The stromal proteinase MMP3/stromelysin-1 promotes mammary carcinogenesis. Cell. 1999; 98: 137–146. https://doi.org/10.1016/s0092-8674(00)81009-0

[17] Correia AL, Mori H, Chen EI, Schmitt FC, Bissell MJ. The hemopexin domain of MMP3 is responsible for mammary epithelial invasion and morphogenesis through extracellular interaction with HSP90β. Genes & Development. 2013; 27: 805–817. https://doi.org/10.1101/gad.211383.112

[18] Mehner C, Miller E, Nassar A, Bamlet WR, Radisky ES, Radisky DC. Tumor cell expression of MMP3 as a prognostic factor for poor survival in pancreatic, pulmonary, and mammary carcinoma. Genes & Cancer. 2015; 6: 480–489. https://doi.org/10.18632/genesandcancer.90

[19] Sympson CJ, Bissell MJ, Werb Z. Mammary gland tumor formation in transgenic mice overexpressing stromelysin-1. Seminars in Cancer Biology. 1995; 6: 159–163. https://doi.org/10.1006/scbi.1995.0022

[20] Lochter A, Galosy S, Muschler J, Freedman N, Werb Z, Bissell MJ. Matrix metalloproteinase stromelysin-1 triggers a cascade of molecular alterations that leads to stable epithelial-to-mesenchymal conversion and a premalignant phenotype in mammary epithelial cells. The Journal of Cell Biology. 1997; 139: 1861–1872. https://doi.org/10.1083/jcb.139.7.1861

[21] Radisky DC, Levy DD, Littlepage LE, Liu H, Nelson CM, Fata JE, et al. Rac1b and reactive oxygen species mediate MMP-3-induced EMT and genomic instability. Nature. 2005; 436: 123–127. https://doi.org/10.1038/nature03688

[22] Caudroy S, Polette M, Nawrocki-Raby B, Cao J, Toole BP, Zucker S, et al. EMMPRIN-mediated MMP regulation in tumor and endothelial cells. Clinical & Experimental Metastasis. 2002; 19: 697–702. https://doi.org/10.1023/a:1021350718226

[23] Banik D, Netherby CS, Bogner PN, Abrams SI. MMP3-mediated tumor progression is controlled transcriptionally by a novel IRF8-MMP3 interaction. Oncotarget. 2015; 6: 15164–15179. https://doi.org/10.18632/oncotarget.3897

[24] Ogata Y, Enghild JJ, Nagase H. Matrix metalloproteinase 3 (stromelysin) activates the precursor for the human matrix metalloproteinase 9. The Journal of Biological Chemistry. 1992; 267: 3581–3584.

[25] Mehner C, Hockla A, Miller E, Ran S, Radisky DC, Radisky ES. Tumor cell-produced matrix metalloproteinase 9 (MMP-9) drives malignant progression and metastasis of basal-like triple negative breast cancer. Oncotarget. 2014; 5: 2736–2749. https://doi.org/10.18632/oncotarget.1932

[26] Vandenbroucke RE, Libert C. Is there new hope for therapeutic matrix metalloproteinase inhibition? Nature Reviews. Drug Discovery. 2014; 13: 904–927. https://doi.org/10.1038/nrd4390

[27] Almutairi S, Kalloush HM, Manoon NA, Bardaweel SK. Matrix Metalloproteinases Inhibitors in Cancer Treatment: An Updated Review (2013-2023). Molecules (Basel, Switzerland). 2023; 28: 5567. https://doi.org/10.3390/molecules28145567

[28] Fields GB. The Rebirth of Matrix Metalloproteinase Inhibitors: Moving Beyond the Dogma. Cells. 2019; 8: 984. https://doi.org/10.3390/cells8090984

[29] Fingleton B. MMPs as therapeutic targets–still a viable option? Seminars in Cell & Developmental Biology. 2008; 19: 61–68. https://doi.org/10.1016/j.semcdb.2007.06.006

[30] Winer A, Adams S, Mignatti P. Matrix Metalloproteinase Inhibitors in Cancer Therapy: Turning Past Failures Into Future Successes. Molecular Cancer Therapeutics. 2018; 17: 1147–1155. https://doi.org/10.1158/1535-7163.MCT-17-0646

[31] Rudzińska M, Daglioglu C, Savvateeva LV, Kaci FN, Antoine R, Zamyatnin AA, Jr. Current Status and Perspectives of Protease Inhibitors and Their Combination with Nanosized Drug Delivery Systems for Targeted Cancer Therapy. Drug Design, Development and Therapy. 2021; 15: 9–20. https://doi.org/10.2147/DDDT.S285852

[32] Shoari A, Rasaee MJ, Kanavi MR, Daraei B. Functional mimetic peptide discovery isolated by phage display interacts selectively to fibronectin domain and inhibits gelatinase. Journal of Cellular Biochemistry. 2019; 120: 19699–19711. https://doi.org/10.1002/jcb.29276

[33] Desmyter A, Spinelli S, Roussel A, Cambillau C. Camelid nanobodies: killing two birds with one stone. Current Opinion

in Structural Biology. 2015; 32: 1–8. https://doi.org/10.1016/j.sbi.2015.01.001

[34] Kim JYJ, Sang Z, Xiang Y, Shen Z, Shi Y. Nanobodies: Robust miniprotein binders in biomedicine. Advanced Drug Delivery Reviews. 2023; 195: 114726. https://doi.org/10.1016/j.addr.2023.114726

[35] Jin BK, Odongo S, Radwanska M, Magez S. NANOBODIES®: A Review of Diagnostic and Therapeutic Applications. International Journal of Molecular Sciences. 2023; 24: 5994. https://doi.org/10.3390/ijms24065994

[36] Blueggel M, Gül D, Stauber RH, Knauer SK. Small but mighty: the versatility of nanobodies in modern medicine. Nanoscale Horizons. 2025; 10: 2158–2171. https://doi.org/10.1039/d5nh00283d

[37] Alexander E, Leong KW. Discovery of nanobodies: a comprehensive review of their applications and potential over the past five years. Journal of Nanobiotechnology. 2024; 22: 661. https://doi.org/10.1186/s12951-024-02900-y

[38] Nam DH, Rodriguez C, Remacle AG, Strongin AY, Ge X. Active-site MMP-selective antibody inhibitors discovered from convex paratope synthetic libraries. Proceedings of the National Academy of Sciences of the United States of America. 2016; 113: 14970–14975. https://doi.org/10.1073/pnas.1609375114

[39] Razai AS, Eckelman BP, Salvesen GS. Selective inhibition of matrix metalloproteinase 10 (MMP10) with a single-domain antibody. The Journal of Biological Chemistry. 2020; 295: 2464–2472. https://doi.org/10.1074/jbc.RA119.011712

[40] Marturano A, Hendrickx MLV, Falcinelli E, Sebastiano M, Guglielmini G, Hassanzadeh-Ghassabeh G, et al. Development of anti-matrix metalloproteinase-2 (MMP-2) nanobodies as potential therapeutic and diagnostic tools. Nanomedicine: Nanotechnology, Biology, and Medicine. 2020; 24: 102103. https://doi.org/10.1016/j.nano.2019.102103

[41] David M, Faihy A, Rolland C, Edir A, Canivet A, Ligat L, et al. Bispecific nanobody® as a new pharmacological drug for the selective inhibition of Trypsin-3. British Journal of Pharmacology. 2025; 182: 4578–4591. https://doi.org/10.1111/bph.70100

[42] McMahon C, Baier AS, Pascolutti R, Wegrecki M, Zheng S, Ong JX, et al. Yeast surface display platform for rapid discovery of conformationally selective nanobodies. Nature Structural & Molecular Biology. 2018; 25: 289–296. https://doi.org/10.1038/s41594-018-0028-6

[43] Skiba MA, Canavan C, Nemeth GR, Liu J, Kanso A, Kruse AC. Epitope-directed selection of GPCR nanobody ligands with evolvable function. Proceedings of the National Academy of Sciences of the United States of America. 2025; 122: e2423931122. https://doi.org/10.1073/pnas.2423931122

[44] Raeeszadeh-Sarmazdeh M, Greene KA, Sankaran B, Downey GP, Radisky DC, Radisky ES. Directed evolution of the metalloproteinase inhibitor TIMP-1 reveals that its N- and C-terminal domains cooperate in matrix metalloproteinase recognition. The Journal of Biological Chemistry. 2019; 294: 9476–9488. https://doi.org/10.1074/jbc.RA119.008321

[45] Angelini A, Chen TF, de Picciotto S, Yang NJ, Tzeng A, Santos MS, et al. Protein Engineering and Selection Using Yeast Surface Display. Methods in Molecular Biology (Clifton, N.J.). 2015; 1319: 3–36. https://doi.org/10.1007/978-1-4939-2748-7_1

[46] Raeeszadeh-Sarmazdeh M, Coban M, Mahajan S, Hockla A, Sankaran B, Downey GP, et al. Engineering of tissue inhibitor of metalloproteinases TIMP-1 for fine discrimination between closely related stromelysins MMP-3 and MMP-10. The Journal of Biological Chemistry. 2022; 298: 101654. https://doi.org/10.1016/j.jbc.2022.101654

[47] Shoari A, Coban MA, Hockla A, Rezhdo A, Dimesa AM, Raeeszadeh-Sarmazdeh M, et al. Directed evolution of metalloproteinase inhibitor TIMP-1 for selective inhibition of MMP-9 exploits catalytic and fibronectin domain interactions. The Journal of Biological Chemistry. 2025; 301: 110258. https://doi.org/10.1016/j.jbc.2025.110258

[48] Piperigkou Z, Mangani S, Kremmydas S, Koletsis NE, Karamanos NK. A guide to the types, structures, and multifaceted functions of matrix metalloproteinases in cancer. The FEBS Journal. 2026; 293: 3717–3757. https://doi.org/10.1111/febs.70296

[49] Quintero-Fabián S, Arreola R, Becerril-Villanueva E, Torres-Romero JC, Arana-Argáez V, Lara-Riegos J, et al. Role of Matrix Metalloproteinases in Angiogenesis and Cancer. Frontiers in Oncology. 2019; 9: 1370. https://doi.org/10.3389/fonc.2019.01370

[50] Levin M, Udi Y, Solomonov I, Sagi I. Next generation matrix metalloproteinase inhibitors - Novel strategies bring new prospects. Biochimica et Biophysica Acta. Molecular Cell Research. 2017; 1864: 1927–1939. https://doi.org/10.1016/j.bbamcr.2017.06.009

[51] Shoari A, Khalili-Tanha G, Coban MA, Radisky ES. Structure and computation-guided yeast surface display for the evolution of TIMP-based matrix metalloproteinase inhibitors. Frontiers in Molecular Biosciences. 2023; 10: 1321956. https://doi.org/10.3389/fmolb.2023.1321956

[52] Kalantar M, Hilpert GA, Mosca ER, Raeeszadeh-Sarmazdeh M. Engineering metalloproteinase inhibitors: tissue inhibitors of metalloproteinases or antibodies, that is the question. Current Opinion in Biotechnology. 2024; 86: 103094. https://doi.org/10.1016/j.copbio.2024.103094

[53] Davydova EK. Protein Engineering: Advances in Phage Display for Basic Science and Medical Research. Biochemistry. Biokhimiia. 2022; 87: S146–S167. https://doi.org/10.1134/S0006297922140127

[54] Hosse RJ, Rothe A, Power BE. A new generation of protein display scaffolds for molecular recognition. Protein Science: a Publication of the Protein Society. 2006; 15: 14–27. https://doi.org/10.1110/ps.051817606

[55] Mulero F, Oteo M, Garaulet G, Magro N, Rebollo L, Medrano G, et al. Development of anti-membrane type 1-matrix metalloproteinase nanobodies as immunoPET probes for triple negative breast cancer imaging. Frontiers in Medicine. 2022; 9: 1058455. https://doi.org/10.3389/fmed.2022.1058455

[56] Demeestere D, Dejonckheere E, Steeland S, Hulpiau P, Haustraete J, Devoogdt N, et al. Development and Validation of a Small Single-domain Antibody That Effectively Inhibits Matrix Metalloproteinase 8. Molecular Therapy: the Journal of the American Society of Gene Therapy. 2016; 24: 890–902. https://doi.org/10.1038/mt.2016.2

[57] Kalantar M, Khorasani Buxton E, Reid KM, Bleyl D, Leitner DM, Raeeszadeh-Sarmazdeh M. Engineering Single-Chain Antibody Fragment (scFv) Variants Targeting A Disintegrin and Metalloproteinase-17 (ADAM-17). Biomolecules. 2025; 16: 31. https://doi.org/10.3390/biom16010031

[58] Rodríguez D, Morrison CJ, Overall CM. Matrix metalloproteinases: what do they not do? New substrates and biological roles identified by murine models and proteomics. Biochimica et Biophysica Acta (BBA) - Molecular Cell Research. 2010; 1803: 39–54. https://doi.org/10.1016/j.bbamcr.2009.09.015

[59] Deu E, Verdoes M, Bogyo M. New approaches for dissecting protease functions to improve probe development and drug discovery. Nature Structural & Molecular Biology. 2012; 19: 9–16. https://doi.org/10.1038/nsmb.2203

[60] Lombard C, Saulnier J, Wallach J. Assays of matrix metalloproteinases (MMPs) activities: a review. Biochimie. 2005; 87: 265–272. https://doi.org/10.1016/j.biochi.2005.01.007

[61] Hotary K, Li XY, Allen E, Stevens SL, Weiss SJ. A cancer cell

metalloprotease triad regulates the basement membrane transmigration program. Genes & Development. 2006; 20: 2673–2686. https://doi.org/10.1101/gad.1451806

[62] Deakin NO, Turner CE. Distinct roles for paxillin and Hic-5 in regulating breast cancer cell morphology, invasion, and metastasis. Molecular Biology of the Cell. 2011; 22: 327–341. https://doi.org/10.1091/mbc.e10-09-0790

[63] Sharabi O, Shirian J, Grossman M, Lebendiker M, Sagi I, Shifman J. Affinity- and specificity-enhancing mutations are frequent in multispecific interactions between TIMP2 and MMPs. PloS One. 2014; 9: e93712. https://doi.org/10.1371/journal.pone.0093712

[64] Batra J, Soares AS, Mehner C, Radisky ES. Matrix metalloproteinase-10/TIMP-2 structure and analyses define conserved core interactions and diverse exosite interactions in MMP/TIMP complexes. PloS One. 2013; 8: e75836. https://doi.org/10.1371/journal.pone.0075836

[65] Wu S, Chen P, Zhou W, Wang H, Song C, Tian Z, et al. Precision targeted therapy and immunotherapy in breast cancer: Advances and clinical frontiers. Chinese Medical Journal. 2026. https://doi.org/10.1097/CM9.0000000000004168 (online ahead of print)